*energies*

*Article*

# Study on a Discharge Circuit Prediction Model of High-Voltage Electro-Pulse Boring Based on Bayesian Fusion

**Changping Li [1,2], Xiaohui Wang [1], Longchen Duan [3] and Bo Lei [1,*]**

1 School of Mechanical Engineering and Electronic Information, China University of Geosciences, Wuhan 430074, China; lichangpingcug@126.com (C.L.); w572883365@126.com (X.W.)
2 Hubei Key Laboratory of Drilling and Production Engineering for Oil and Gas, Yangtze University, Wuhan 430199, China
3 Faculty of Engineering, China University of Geosciences, Wuhan 430074, China; duanlongchencug@163.com
* Correspondence: leizh@cug.edu.cn; Tel.: +86-177-6259-0086

**Abstract:** It is necessary to develop new drilling and breaking technology for hard rock construction. However, the process of high-voltage electro-pulse (HVEP) rock-breaking is complex, and the selection of electro-pulse boring (EPB) process parameters lacks a theoretical basis. Firstly, the RLC model, TV-RLC model, and TV-CRLC model are established based on the characteristics of the HVEP circuit to predict the EPB dynamic discharge curve. Secondly, the parameters are identified by the Particle Swarm Optimization Genetic Algorithm (PSO-GA). Finally, due to the nonlinear and complex time-varying characteristics of the discharge circuit, the discharge circuit prediction models based on Bayesian fusion and current residual normalization fusion method are proposed, and the optimal weight of these three models is determined. Compared with the single models for EPB current prediction, the average relative error reduction rates based on Bayesian fusion and current residual normalization fusion methods are 25.5% and 9.5%, respectively. In this paper, the discharge circuit prediction model based on Bayesian fusion is established, which improves the prediction accuracy and reliability of the model, and it guides the selection of process parameters and the design of pulse power supply and electrode bits.

**Keywords:** electro-pulse boring; bayes; model fusion; parameter identification; prediction model

check for updates

**Citation:** Li, C.; Wang, X.; Duan, L.; Lei, B. Study on a Discharge Circuit Prediction Model of High-Voltage Electro-Pulse Boring Based on Bayesian Fusion. *Energies* **2022**, *15*, 3824. https://doi.org/10.3390/en15103824

Academic Editor: Hossein Hamidi

Received: 21 April 2022
Accepted: 13 May 2022
Published: 23 May 2022



## 1. Introduction

Deep resources exploitation mostly depends on deep and ultra-deep well technology [1]. To avoid bit loosening or loss, traditional rotary drilling requires frequent lifting in drilling deep wells, which wastes time and incurs high costs. For example, it takes about 10 h to pull the drill string in drilling a 3000 m deep well. At the same time, the drilling and blasting method is often used for hard rock breaking in the construction of deep foundation pits and tunnel sections. Drilling and blasting methods have some disadvantages, such as serious disturbance and damage to surrounding rock, great environmental pollution, and great impact on surrounding buildings [2]. Therefore, it is necessary to develop new breaking technology for hard rock. HVEP rock-breaking technology, with the characteristics of controllable energy and high rock breaking efficiency, has been proved to be feasible in the research [3,4]. Usov et al. [5] compared the energy loss of the existing rock-breaking drilling methods in the drilling process and found that the specific energy for HVEP breaking was 100–300 J/cm$^3$. Compared with the specific energy of the water jet (1000–2000 J/cm$^3$) and laser drilling (5000–12,000 J/cm$^3$), the specific energy of HVEP rock-breaking was lower. Meanwhile, tensile stress could be produced in HVEP rock-breaking processes, which introduced great advantages in hard rock drilling. Schiegg et al. [4] compared the costs of mechanical rotary drilling and high-voltage EPB and found that the rotary drilling cost exceeded 2000 EUR/m when drilling depth exceeded 5 km. When the depth exceeded 8 km, the cost of rotary drilling exceeded 30,000 EUR/m. Nevertheless, the cost of high-voltage

EPB was still about 100 EUR/m, which was not limited by the required drilling depth. Therefore, HVEP rock-breaking has broad application prospects in the aspects hard rock drilling relative to deep and ultra-deep wells and hard rock excavation of large sectioned tunnels. However, the process of HVEP rock-breaking is complex, and electrode bit designs and EPB process parameter selection lack a theoretical basis, which impede the engineering process of HVEP rock-breaking [6,7]. Meanwhile, physical-mathematical models do not accurately predict real-time parameters and the crushing effect of the HVEP rock-breaking process [8].

With respect to the HVEP rock-breaking prediction model, Zhu et al. [9] used discrete element software PFC to study the rock electric fracture process and adopted the dielectric breakdown model (DBM) to discuss factors affecting the development of plasma channel and established a numerical model of rock fracture in consideration of three fields of electricity, heat, and force. Zhu et al. [10] proposed a new model of rock dielectric breakdown with a probability development model (PDM) based on energy conversion efficiency. Burkin et al. [11,12] established the models of the electric explosion to analyze the relationship between discharge circuit parameters and wave power characteristics. Walsh and Vogler [13] adopted Moose software to simulate the flow channel of pulse currents in rock and a new method to simulate the electric fragmentation of rock was proposed. The method was divided into two stages. Firstly, the electric breakdown of rock was simulated by tracking resistance heating and increasing conductivity. Then, the heating effect was simulated by the thermo-mechanical response in rocks. Lopatin et al. [14] and Usmanov et al. [15] built the mathematical models based on the stochastic deterministic method, the voltage and current characteristics of the breakdown process were obtained. Kuznetsova et al. [16] established a physical and mathematical model of HVEP rock-breaking, which described the operation of discharge circuit, the expansion of the plasma channel. Hu [17] established an energy transfer model to analyze energy injection and consumption processes. The solid-state pulse power supply with 100 ns rise time was developed. Li et al. [18] established a mathematical model of HVEP breaking and simulated and analyzed the influence of continuous change in discharge parameters on high-voltage EPB. Due to the on–off time delay of the gas discharge switch in the HVEP rock-breaking test system, Li et al. [19] established a discharge model based on variable resistance in the circuit. EPB tests and electric parameter curve acquisition in different rock samples were carried out, and then the least square method was adopted to identify model parameters, and the parameters of the discharge circuit model in different rock samples were obtained. In conclusion, the established prediction model of HVEP rock-breaking is based on commercial software or a single physical and mathematical model, and the prediction accuracy of the model still has great room for improvement.

In consideration of the on–off time delay of the discharge switch and the stray capacitance in EPB circuit with steep front waveform, the discharge circuit prediction model including the RLC, TV-RLC, and TV-CRLC models was established. The parameters of these three models were identified and the discharge process curve was fitted. Compared with the test curves collected during EPB rock-breaking in granite and red sandstone, the error characteristics of each model in the discharge process parameter prediction were analyzed. Due to the nonlinear and complex time-varying characteristics of a high-voltage pulse discharge circuit, the prediction method based on a single equivalent circuit model cannot accurately predict discharge process parameters. A discharge circuit prediction model of EPB rock-breaking based on Bayesian fusion is proposed to improve the practical application performance of the prediction model. In particular, the probability method based on the Bayesian theorem is used to obtain the models' weight, and it is then compared with the current residual normalization fusion method for prediction effects. The accuracy improvement rate of the discharge circuit prediction model based on Bayesian fusion is verified. By conducting research, the selection and design of pulse power supplies, EPB bit, and EPB process parameters can be guided.

## 2. Prediction Model of Discharge Circuit in EPB

According to the characteristics of discharge circuit in EPB process, the prediction model of discharge circuits in high-voltage EPB rock-breaking based on constant resistance (RLC model for short), the prediction model of discharge circuit in high-voltage EPB rock-breaking based on time-varying resistance (TV-RLC model for short), and the prediction model of discharge circuit in high-voltage EPB rock-breaking based on time-varying resistance and distributed capacitance (TV-CRLC model for short) were built. The equivalent circuits of these three models are shown in Figure 1.

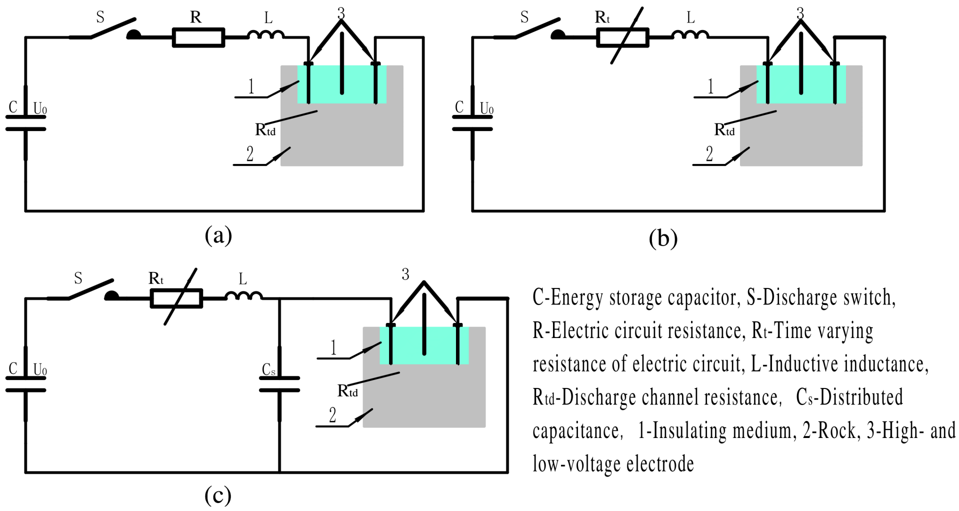


**Figure 1.** EPB Equivalent circuits of these three models, (**a**) RLC equivalent circuit model, (**b**) TV-RLC equivalent circuit model, and (**c**) TV-CRLC equivalent circuit model.

### *2.1. RLC Model*

EPB discharge system can be equivalent to the circuit shown in Figure 1a, the following equation can be obtained based on the Kirchhoff voltage law:

$$U_c(t) + L \times \frac{di}{dt} + (R + R_{td}) \times i(t) = 0 \tag{1}$$

where symbol $i$ represents the current in the loop for capacitor $C$.

$$C \times \frac{dU_c(t)}{dt} = i(t) \tag{2}$$

The direction of charging voltage $U_0$ is opposite to the direction of the discharge voltage. The following results can be obtained by integrating both sides.

$$U_c = \frac{1}{C}\int_0^t i(t)dt - U_0 \tag{3}$$

The Weizel–Rompe model [20–23] was adopted for the discharge channel impedance model, and it can be expressed with the following formula:

$$R_{td}(t) = \frac{K_{td} \times l_{td}}{\sqrt{(\int_0^t i^2(t)dt)}} \tag{4}$$

where $K_{td}$ and $l_{td}$ represent the resistance coefficient and the discharge channel length respectively. In this model, the equations can be solved simultaneously by using variable-order differential equations.

*2.2. TV-RLC Model*

A gas discharge switch has time delay characteristics during on-off. After the gas switch turns on, the electrical circuit's resistance drops rapidly [24], and the resistance model can be expressed with the following formula:

$$R_t = R_1 + (R_0 - R_1)e^{\frac{-t}{\theta_R}} \tag{5}$$

where symbols $R_0$, $R_1$, and $\theta_R$ represent initial resistance, limit minimum resistance, and resistance drop time constant, respectively.

According to the equivalent circuit and Kirchhoff circuit equation in Figure 1b, the following formula can be obtained.

$$U_c(t) + L \times \frac{di}{dt} + (R_t + R_{td}) \times i(t) = 0 \tag{6}$$

The equations in the model can also be solved simultaneously by solving variable-order differential equations.

*2.3. TV-CRLC Model*

The pulse voltage with an increasing edge that is less than 500 ns is a prerequisite for HVEP rock-breaking [25–28], so it can achieve HVEP rock-breaking instead of hydro-electric rock-breaking. To induce a fast leading edge in the output high-voltage pulse of the pulse power supply, one of the essentials is to decrease the loop inductance. At the same time, the favorable distributed capacitance in the loop should be rationally used and the unfavorable distributed capacitance should be eliminated [29,30] to generate higher overvoltage at both ends of the discharge switch and to rapidly conduct the switch. It is ensured that the establishment process of the steep front waveform is not affected by the slow action of the switch. The following equation can be obtained from the equivalent circuit in Figure 1c and the Kirchhoff circuit equation:

$$U_c(t) + U_{R_t}(t) + U_L(t) + U_{td}(t) = 0 \tag{7}$$

where $U_c(t)$ is the capacitor voltage, $U_{R_t}(t)$ is the voltage of $R_t$, and $U_L(t)$ is the voltage of $L$. $U_{td}(t)$ is the voltage on both sides of $C_s$, which can be expressed as:

$$U_{td}(t) = (i - C_s \frac{dU_{td}}{dt}) \times R_{td} \tag{8}$$

The equations in the model can also be solved simultaneously by the finite element method.

## 3. Parameter Identification and Bayesian Fusion Algorithm

*3.1. Parameter Identification for the Prediction Model*

According to these three prediction models of the EPB process, the parameters to be identified include dispersion capacitance $c_s$, inductance $l$, electric circuit resistance $r$, initial impedance $r_0$, minimum limit resistance $r_1$ and resistance drop time constant $\theta_r$, plasma channel length $l_{td}$, and resistance coefficient $k_{td}$. Combined with the variable order differential equation method and finite element method, the parameters of these three models were identified by PSO-GA. In the hybrid intelligent algorithm of PSO-GA, the solution space is used for real number coding, and the roulette algorithm [31,32] is used. The fitness function is established in this algorithm, which refers to the simulated annealing process [33].

$$f(x_i) = e^{-beta \times pcost} \tag{9}$$

where $f(x_i)$, *beta* and *pcost* represent the fitness function value of Individual $i$, the exponential coefficient and the error, respectively.

The hybrid intelligent algorithm of PSO-GA for parameter identification includes three parts: the first one is initialization, the second one is GA identification, and the third one is PSO identification. Firstly, the learning factor, crossover probability, and other coefficients such as particle position, velocity, and other space were initialized in the hybrid intelligent algorithm of PSO-GA. The PSO is used to traverse all particles, and the parameters to be identified are obtained as the initial values. Secondly, the GA is run. When the evolution times are less than the maximum evolution times, the genetic evolution is continued. Finally, the particle velocity and position are updated in the range of iterations, and the individual optimal value and global optimal value are updated until the maximum number of iterations is reached, and the parameter value corresponding to the minimum relative error is returned.

### *3.2. Fusion Algorithm based on Bayesian Theorem*

To improve the prediction accuracy of high-voltage pulse discharge circuit parameters, a fusion method for the multi prediction model was proposed. As shown in Figure 2, the multi-model fusion framework of discharge circuits for high-voltage EPB rock-breaking is presented. After filtering and identifying the parameters of high-voltage EPB process, parameter identification array $\tilde{z}_j$ is obtained. Symbol $j$ is the number of the parameters to be identified. The values are 5, 6, and 7 for the RLC model, TV-RLC model, and TV-CRLC model, respectively. Then, according to the predicted current as the basis of fusion, the parameters of the high voltage pulse discharge process can be predicted by weighing the fusion module.

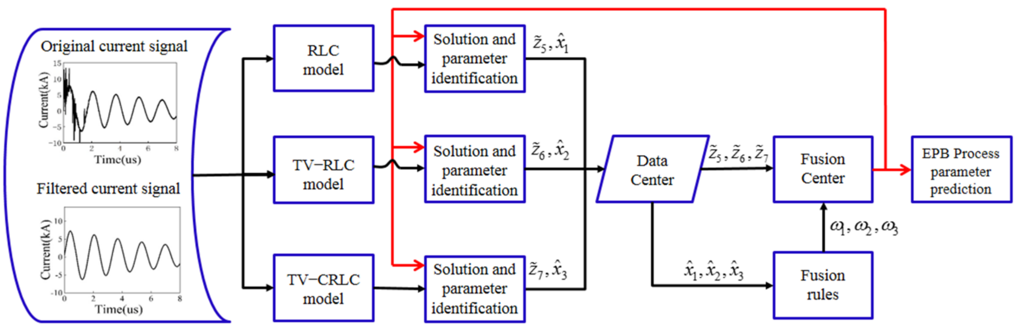


**Figure 2.** Multi-model fusion framework of discharge circuit for high-voltage EPB rock-breaking.

The result of model fusion prediction is the weighted value of the real-time prediction results of each model. Equation (10) can be obtained, where $\hat{x}_1$, $\hat{x}_2$, and $\hat{x}_3$ are the current prediction values of the RLC model, TV-RLC model, and TV-CRLC model, respectively:

$$\hat{x}_{fn} = \omega_1 \hat{x}_1 + \omega_2 \hat{x}_2 + \omega_3 \hat{x}_3 \tag{10}$$

where $\omega_i$ is the fusion weight, and the sum of the weights is 1. The core of the fusion algorithm is to determine the weight of each model. The weight of the model can be obtained by using the residual current and Bayesian theory. By conductin a comparative analysis of the current curve predicted by different fusion methods and the actual current curve, the fusion method suitable for the prediction model of high-voltage EPB rock-breaking was obtained. The error can reflect similarities between the prediction current and the actual discharge current.

$$E_i(k) = x(k) - \hat{x}(k) \tag{11}$$

Symbol $E_i(k)$ represents the current error, $x(k)$ and $\hat{x}(k)$ represent the actual and predicted current value at Moment $k$ respectively. The current residuals of different models are normalized to obtain the performance index function [34,35], as shown in Equation (12):

$$\omega_i(k) = \frac{S(k) - E_i^2(k)}{2 \times S(k)} \tag{12}$$

where $S(k) = \sum\limits_{i=1}^{3} E_i^2(k)$, and $\omega_i(k)$ is the weight value of $i$-th model. The weight of each model can be obtained by using the current's residual. The more accurate the model prediction value, the smaller the corresponding residual error, and the larger the corresponding weight value.

Meanwhile, the probability can be used to describe the closeness between the predicted and actual current value in different models at a certain time. According to the Bayesian theory [36,37], the following equations can be obtained.

$$P(p_i|x(k)) = \frac{f(x(k)|p_i)P(p_i)}{\sum\limits_{i=1}^{3} f(x(k)|p_i)P(p_i)} \tag{13}$$

$$P(p_i|x(k-1)) = \frac{P(x(k-1)|p_i)P(p_i)}{P(x(k-1))} \tag{14}$$

Because $P(x(k-1)|p_i) = P(x(k-1))$ is a certain event, its probability is 1. Formula (12) can be expressed as follows.

$$\omega_i(k) = P(p_i|x(k)) = \frac{f(x(k)|p_i)P(p_i|x(k-1))}{\sum\limits_{i=1}^{3} f(x(k)|p_i)P(p_i|x(k-1))} \tag{15}$$

The weight of each model can be obtained by using Formula (15), and the real-time predicted value can be obtained by using Formula (10).

## 4. Results and Discussion

### *4.1. High-Voltage EPB Process Test*

High-voltage EPB rock-breaking experiments were conducted in red sandstone and granite, and the real-time current parameters of the EPB process were collected. The schematic diagram of the high-voltage EPB rock-breaking test system is shown in Figure 3. The transformer boost type pulse power supply is adopted for the EPB test system. The energy storage capacitor and maximum storage energy are 20 nF and 400 J, respectively [38]. The output peak voltage is 200 kV, and the step-up ratio of the transformer is 1:40. EPB experiment system can achieve EPB experiment and electric parameter detection experiment in different rock samples. Rogowski coil and RTD1004 oscilloscope are used to detect the current parameters in the EPB process.

It has a great interference on the collected current signal. The current signals in different rock samples are collected by the electrical parameter detection subsystem. Consequently, it is essential to use a software algorithm to filter the current signals in order to extract and analyze the current signals of different rock samples. Under the intense interference of the pulse power supply, the filtering performance of traditional filtering algorithms [39,40] is restricted. Singular value decomposition (SVD) filtering algorithm has an excellent filtering effect [41,42]. Before SVD filtering denoising, it is necessary to construct the matrix of the original current signal collected by the electrical parameter detection subsystem, including the Toeplitz matrix and Hankel matrix [43,44]. Toeplitz matrix can helps speed up the filtering process. A SVD filtering algorithm based on the Toeplitz matrix is proposed. The original and filtered signals are shown in Figure 4.

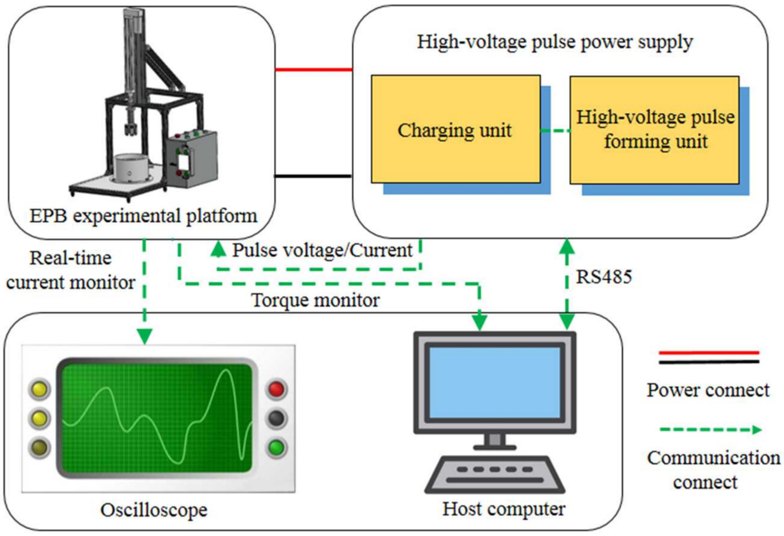


**Figure 3.** Schematic diagram of EPB test system.

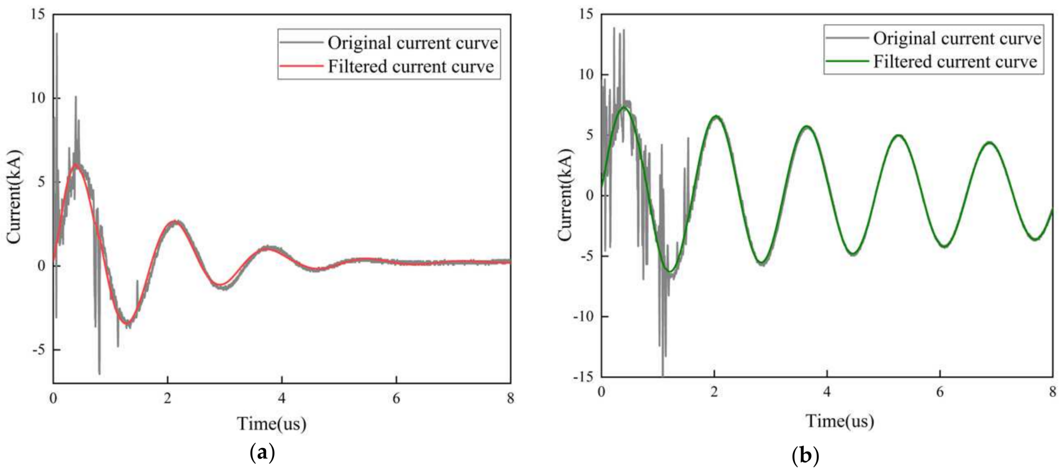


**Figure 4.** Original signals and filtered curves: (**a**) red sandstone and (**b**) granite.

### *4.2. Parameter Identification Results of EPB Prediction Model*

The parameters of the RLC, TV-RLC, and TV-CRLC model are identified by PSO-GA. When the models with identified parameters are used to predict the EPB process curve, the error between the predicted and experimental current values is minimized, and the objective function is globally optimal. With EPB current curves in red sandstone and granite as the model prediction target, the identified parameters of different models are obtained, as shown in Table 1. The resistance coefficient $K_{td}$ of granite increases and the length of plasma channel $l_{td}$ shortens compared with red sandstone.

The identified parameters are substituted into each model. As shown in Figure 5, the current prediction curve of different circuit models and the test curves of high-voltage EPB were compared. The overall prediction accuracy of the TV-CRLC model is the highest, followed by the TV-RLC model, and then the RLC model. This means that the weight of the TV-CRLC model is higher when Bayesian fusion is adopted. Different models have different prediction accuracy distribution in different time intervals. The difference of models directly affects the prediction accuracy, so the model fusion is required to improve the parameter prediction accuracy in the high-voltage EPB rock-breaking process.

**Table 1.** Parameter identification results of RLC, TV-RLC, and TV-CRLC model.

| Model | Red Sandstone | Granite |
| --- | --- | --- |
| RLC | $L = 3.47$ µH<br>$R = 4.07\ \Omega$<br>$l_{td} = 19.72$ mm<br>$K_{td} = 125.38\ \mathrm{V} \cdot \mathrm{S}^{1/2}/\mathrm{m}$ | $L = 3.28$ µH<br>$R = 0.54\ \Omega$<br>$l_{td} = 10.1$ mm<br>$K_{td} = 200.76\ \mathrm{V} \cdot \mathrm{S}^{1/2}/\mathrm{m}$ |
| TV-RLC | $L = 3.4$ µH<br>$R_0 = 1.7$ M$\Omega$<br>$R_1 = 3.4\ \Omega$<br>$\theta_R = 3.0 \times 10^{-9}$<br>$l_{td} = 27.1$ mm<br>$K_{td} = 189.9\ \mathrm{V} \cdot \mathrm{S}^{1/2}/\mathrm{m}$ | $L = 3.3$ µH<br>$R_0 = 4.1$ M$\Omega$<br>$R_1 = 0.02\ \Omega$<br>$\theta_R = 1.0 \times 10^{-10}$<br>$l_{td} = 19.8$ mm<br>$K_{td} = 272\ \mathrm{V} \cdot \mathrm{S}^{1/2}/\mathrm{m}$ |
| TV-CRLC | $L = 3.352$ µH<br>$R_0 = 1.7$ M$\Omega$<br>$R_1 = 0.34\ \Omega$<br>$\theta_R = 3.3415 \times 10^{-10}$<br>$l_{td} = 40.4$ mm<br>$K_{td} = 240.805\ \mathrm{V} \cdot \mathrm{S}^{1/2}/\mathrm{m}$<br>$C_s = 0.2$ nF | $L = 3.3139$ µH<br>$R_0 = 2.65$ M$\Omega$<br>$R_1 = 0.002\ \Omega$<br>$\theta_R = 3.6826 \times 10^{-12}$<br>$l_{td} = 11.8$ mm<br>$K_{td} = 317.4474\ \mathrm{V} \cdot \mathrm{S}^{1/2}/\mathrm{m}$<br>$C_s = 3.5341$ nF |

### *4.3. Model Fusion Results of EPB Prediction Model*

The current curves predicted by different models and different fusion methods are shown in Figure 5. The legends of RLC, TV-RLC, and TV-CRLC represent the prediction current curves of the high-voltage EPB based on a single model. The legend normalized fusion represents the current prediction result based on the current residual normalized fusion method. The legend Bayesian fusion represents the current prediction results of the proposed method based on Bayesian fusion. It is evident from the enlarged figure in Figure 5a(A) for the current prediction curve of red sandstone that TV-CRLC prediction accuracy is higher at this stage, and its weight value is larger when the model is fused. In view of the enlarged Figure 5a(B) of the red sandstone current prediction curve, the current prediction accuracy of Bayesian fusion is the highest, followed by normalized fusion, and then TV-CRLC at this stage. Observed from an enlarged Figure 5b(A) of granite current prediction curves, Bayesian fusion and TV-RLC on the left side of the peak have the same prediction accuracy at this stage, Bayesian fusion and TV-CRLC on the right side of the peak have the same prediction accuracy, and the Bayesian fusion method has the highest current prediction accuracy at this stage. As seen from an enlarged Figure 5b(B) of the granite current prediction curve, TV-RLC on the left side of the trough has higher prediction accuracy, while Bayesian fusion and TV-CRLC on the right side of the trough have higher prediction accuracy.

The relative error percentage is used for error analysis to evaluate the single model and the fusion method [45,46]. Table 2 shows the relative error reduction rate of EPB current prediction value using the model fusion methods compared with the single model method. The EPB current prediction accuracy of the Bayesian fusion method is the highest. Compared with a single model for EPB current prediction, the maximum relative error reduction rate by the Bayesian fusion method is 44.3% and the minimum relative error reduction rate is 10.4%. In EPB in red sandstone, the average error reduction rate by the Bayesian fusion method is 32.9%. In EPB in granite, the average error reduction rate of the Bayesian fusion method is 18.1%. However, the average error reduction rate is 14.2% and 4.8%, respectively, when the normalized fusion method based on current residuals is used for the current prediction of EPB in red sandstone and granite. In EPB in granite, compared with the TV-CRLC single model for EPB current prediction, the relative error reduction rate of the current residual normalized fusion method is −4.1%, which means that the prediction accuracy of the current residual normalization method is lower than that of the TV-CRLC model. In conclusion, the prediction accuracy of EPB currents based on the Bayesian fusion method is higher than the one based on the current residual normalization fusion method. All in all, the model fusion method has higher prediction accuracy compared with the single model.

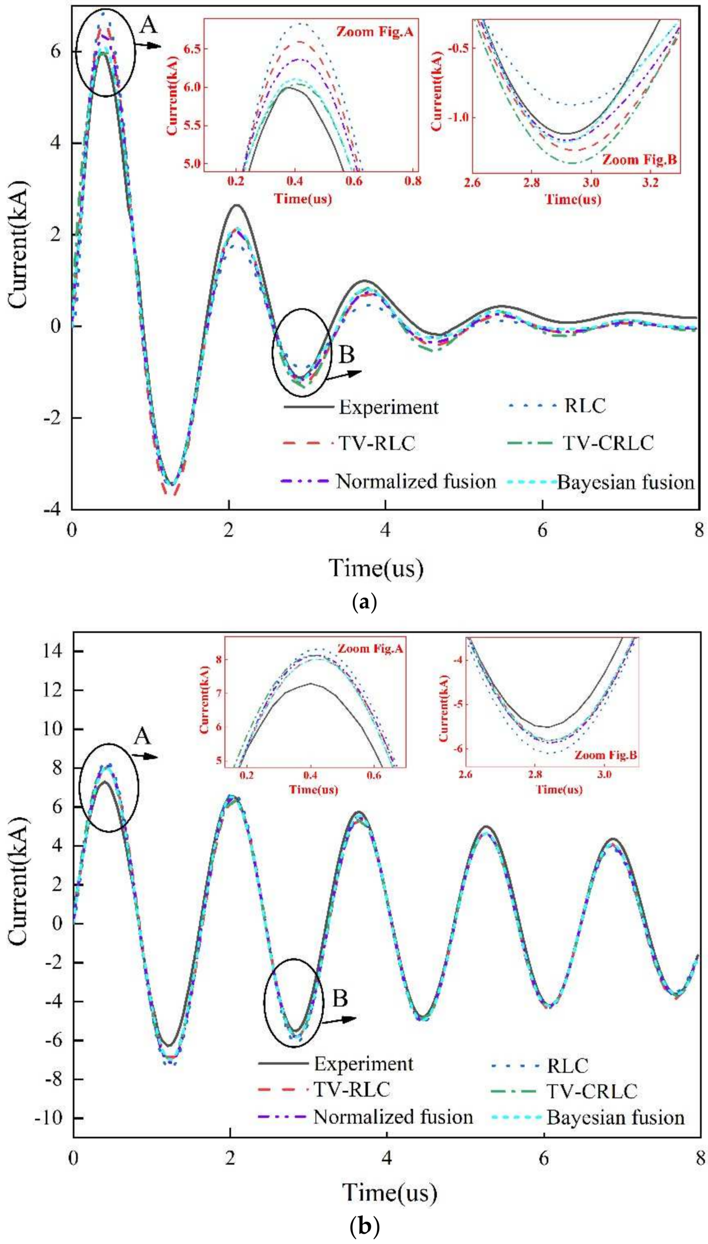


**Figure 5.** Comparison of current prediction curves of different circuit models and fusion models and test curves for high-voltage EPB: (**a**) red sandstone and (**b**) granite.

**Table 2.** Relative error reduction rate of EPB current prediction of different single models and model fusion methods.

| Rock Samples | Model | vs. RLC | vs. TV-RLC | vs. TV-CRLC | Average Reduction Rate |
|---|---|---|---|---|---|
| Red sandstone | Bayesian fusion | 44.3% | 30.3% | 24% | 32.9% |
| | Normalized fusion | 28.8% | 11% | 2.9% | 14.2% |
| Granite | Bayesian fusion | 28.4% | 15.4% | 10.4% | 18.1% |
| | Normalized fusion | 16.8% | 1.7% | −4.1% | 4.8% |

## 5. Conclusions

RLC, TV-RLC, and TV-CRLC models are established in consideration of the time delay and the stray capacitance. Based on the nonlinear and complex time-varying characteristics of high-voltage discharge circuits, the prediction model of EPB rock-breaking based on Bayesian fusion is presented. The predicted current results are compared with the current curves collected from the EPB test, the predicted current curve of the single model, and the predicted curve based on the current residual normalization fusion method.

1. The parameters of the RLC, TV-RLC, and TV-CRLC model are identified by PSO-GA. There is a bigger resistance coefficient and a smaller coefficient length parameter of the plasma channel of granite by EPB in comparison with the ones of red sandstone by EPB. The identified parameters are within a reasonable range and are consistent with the actual EPB effects. At the same time, the effective drilling of red sandstone and granite is realized by conducting the EPB experiment.
2. TV-CRLC model has the highest prediction accuracy for EPB current, followed by the TV-RLC model, and then the RLC model. The weight of the TV-CRLC model is higher when Bayesian fusion is used for current prediction. Different models have different prediction accuracy distribution in different time intervals. Model fusion is applied to improve the prediction accuracy of process parameters in high-voltage EPB rock-breaking.
3. The prediction accuracy based on the Bayesian fusion method is more accurate than that based on the normalization fusion method. Meanwhile, the model fusion method has higher prediction accuracies compared with the single model for EPB process parameters prediction. Compared with the single models for EPB current prediction, the average relative error reduction rate based on Bayesian fusion and current residual normalization fusion method is 25.5% and 9.5%, respectively. The validity of the discharge circuit prediction model based on Bayesian fusion is proved.

**Author Contributions:** Conceptualization, B.L. and L.D.; data curation, B.L. and X.W.; formal analysis, B.L. and X.W.; methodology, C.L. and X.W.; project administration, C.L.; software, C.L.; writing—original draft, C.L. All authors have read and agreed to the published version of the manuscript.

**Funding:** This work was supported by the National Natural Science Foundation of China (42002310) and the Open Fund of Hubei Key Laboratory of Drilling and Production Engineering for Oil and Gas (Yangtze University) (YQZC202207).

**Institutional Review Board Statement:** Not applicable.

**Informed Consent Statement:** Not applicable.

**Data Availability Statement:** Not applicable.

**Acknowledgments:** Thanks to He Mengbing in Huazhong University of Science and Technology for providing the high-voltage pulse power supply in the process of EPB experiment.

**Conflicts of Interest:** The authors declare no conflict of interest.

## References

1. Diaz, M.B.; Kim, K.Y.; Shin, H.; Zhuang, L. Predicting rate of penetration during drilling of deep geothermal well in Korea using artificial neural networks and real-time data collection. *J. Nat. Gas. Sci. Eng.* **2019**, *67*, 225–232. [CrossRef]
2. Wu, F.; Fan, X.; Liu, J.; Li, X. Analytical interpretation of hydraulic fracturing initiation pressure and breakdown pressure. *J. Nat. Gas. Sci. Eng.* **2020**, *76*, 103185. [CrossRef]
3. Rossi, E.; Adams, B.; Vogler, D.; Rudolf Von Rohr, P.; Kammermann, B.; Saar, M.O. Advanced drilling technologies to improve the economics of deep geo-resource utilization. In Proceedings of the 2nd Applied Energy Symposium: MIT A+ B (MITAB 2020) (virtual), 2020, ETH Zurich, Geothermal Energy & Geofluids, Cambridge, MA, USA, 14–18 August 2020; p. 148.
4. Schiegg, H.O.; Rødland, A.; Zhu, G.; Yuen, D.A. Electro-pulse-boring (EPB): Novel super-deep drilling technology for low cost electricity. *J. Earth Sci. China* **2015**, *26*, 37–46. [CrossRef]
5. Usov, A.; Tsukerman, V.; Potokin, A.; Ilin, D. The experience in development of technique and technology of electric pulse disintegration of rocks and ores. In *REWAS 2016*; Springer: Berlin/Heidelberg, Germany, 2016; pp. 325–332.

6. Kusaiynov, K.; Nussupbekov, B.R.; Shuyushbayeva, N.N.; Tanasheva, N.K.; Shaimerdenova, K.M.; Khassenov, A.K. On electric-pulse well drilling and breaking of solids. *Tech. Phys.* **2017**, *62*, 867–870. [CrossRef]
7. Yudin, A.S.; Zhurkov, M.Y.; Martemyanov, S.M.; Datskevich, S.Y.; Vazhov, V.F. Electrical discharge drilling of granite with positive and negative polarity of voltage pulses. *Int. J. Rock Mech. Min.* **2019**, *123*, 104058. [CrossRef]
8. Kuznetsova, N.S.; Lopatin, V.V.; Yudin, A.S. Effect of Electro-Discharge Circuit Parameters on the Destructive Action of Plasma Channel in Solid Media. *J. Phys. Conf. Ser.* **2014**, *552*, 012029. [CrossRef]
9. Zhu, X.; Luo, Y.; Liu, W. On the rock-breaking mechanism of plasma channel drilling technology. *J. Petrol. Sci. Eng.* **2020**, *194*, 107356. [CrossRef]
10. Zhu, X.; Luo, Y.; Liu, W.; He, L.; Gao, R.; Jia, Y. On the Mechanism of High-Voltage Pulsed Fragmentation from Electrical Breakdown Process. *Rock Mech. Rock Eng.* **2021**, *54*, 4593–4616. [CrossRef]
11. Burkin, V.V.; Kuznetsova, N.S.; Lopatin, V.V. Dynamics of electro burst in solids: I. Power characteristics of electro burst. *J. Phys. D Appl. Phys.* **2009**, *42*, 185204. [CrossRef]
12. Burkin, V.V.; Kuznetsova, N.S.; Lopatin, V.V. Dynamics of electro burst in solids: II. Characteristics of wave process. *J. Phys. D Appl. Phys.* **2009**, *42*, 235209. [CrossRef]
13. Walsh, S.D.; Vogler, D. Simulating electropulse fracture of granitic rock. *Int. J. Rock Mech. Min.* **2020**, *128*, 104238. [CrossRef]
14. Lopatin, V.V.; Noskov, M.D.; Usmanov, G.Z.; Cheglokov, A.A. Modeling of impulse electric discharge propagation in a condensed dielectric. *Russ Phys. J.* **2006**, *49*, 243–250. [CrossRef]
15. Usmanov, G.Z.; Lopatin, V.V.; Noskov, M.D.; Cheglokov, A.A. Simulation of electrical discharge development at interface of solid and liquid dielectric. *Izv. Vyssh. Uchebn. Zaved. Fiz.* **2006**, *10*, 231–234.
16. Kuznetsova, N.S.; Yudin, A.S.; Voitenko, N.V. Simulation of Pre-Breakdown Phase of Electrical Discharge in Reinforced Concrete. *J. Phys. Conf. Ser.* **2017**, *830*, 012046. [CrossRef]
17. Hu, Q. Experimental Researches on Pulse Plasma Discharge for Deep-Ocean Thin-Layer Mineral Resources Crushing. *Thalass. Int. J. Mar. Sci.* **2019**, *35*, 405–412. [CrossRef]
18. Li, C.; Duan, L.; Tan, S.; Chikhotkin, V. Influences on High-Voltage Electro Pulse Boring in Granite. *Energies* **2018**, *11*, 2461. [CrossRef]
19. Li, C.; Duan, L.; Wu, L.; Tan, S.; Zheng, J.; Chikhotkin, V. Optimization of discharge circuit model based on electro pulse boring experiment. *J. Nat. Gas. Sci. Eng.* **2021**, *86*, 103730. [CrossRef]
20. Burkin, V.V.; Kuznetsova, N.S.; Lopatin, V.V. Wave dynamics of electric explosion in solids. *Tech. Phys.* **2009**, *54*, 644–650. [CrossRef]
21. Kuznetsova, N.; Lopatin, V.; Burkin, V.; Golovanevskiy, V.; Zhgun, D.; Ivanov, N. Theoretical and experimental investigation of electro discharge destruction of non-conducting materials. In Proceedings of the 2011 IEEE Pulsed Power Conference, Chicago, IL, USA, 19–23 June 2011; pp. 267–273.
22. Li, C.; Duan, L.; Tan, S.; Chikhotkin, V.; Fu, W. Damage Model and Numerical Experiment of High-Voltage Electro Pulse Boring in Granite. *Energies* **2019**, *12*, 727. [CrossRef]
23. Takaki, K.; Akiyama, H. The resistance of a high-current pulsed discharge in nitrogen. *Jpn. J. Appl. Phys.* **2001**, *40*, 979. [CrossRef]
24. Usmanov, G.Z.; Lopatin, V.V.; Noskov, M.D.; Cheglokov, A.A. Mathematical modeling of the solid dielectric brittle destruction as a result of pulse electrical breakdown. In Proceedings of the 15th International Symposium on High-Current Electronics, Tomsk, Russia, 21–26 September 2008.
25. Biela, J.; Marxgut, C.; Bortis, D.; Kolar, J.W. Solid state modulator for plasma channel drilling. *IEEE Trans. Dielectr. Electr. Insul.* **2009**, *16*, 1093–1099. [CrossRef]
26. Gao, Y.; Zhang, S.; Sun, H.; Wang, R.; Tu, X.; Shao, T. Highly efficient conversion of methane using microsecond and nanosecond pulsed spark discharges. *Appl. Energy* **2018**, *226*, 534–545. [CrossRef]
27. Hobejogi, T.; Biela, J. Performance Evaluation of Pulse Compressor-Based Modulators with Very Fast Rise Times for Plasma Channel Drilling. *IEEE Trans. Plasma Sci.* **2014**, *42*, 2891–2898. [CrossRef]
28. Wang, X.; Gao, Y.; Zhang, S.; Sun, H.; Li, J.; Shao, T. Nanosecond pulsed plasma assisted dry reforming of CH4: The effect of plasma operating parameters. *Appl. Energ* **2019**, *243*, 132–144. [CrossRef]
29. Gao, J.; Liu, Y.; Liu, J.; Yang, J.; Zhang, J. Development of a repetitive wave erection Marx generator. *IEEE Trans. Plasma Sci.* **2009**, *37*, 1936–1942.
30. Jia, K.; Li, Y.; Fang, Y.; Zheng, L.; Bi, T.; Yang, Q. Transient current similarity based protection for wind farm transmission lines. *Appl. Energy* **2018**, *225*, 42–51. [CrossRef]
31. Chatterjee, S.; Bandopadhyay, S.; Machuca, D. Ore grade prediction using a genetic algorithm and clustering based ensemble neural network model. *Math. Geosci.* **2010**, *42*, 309–326. [CrossRef]
32. Fernández Álvarez, J.P.; Fernández Martínez, J.L.; Menéndez Pérez, C.O. Feasibility analysis of the use of binary genetic algorithms as importance samplers application to a 1-D DC resistivity inverse problem. *Math. Geosci.* **2008**, *40*, 375–408. [CrossRef]
33. Bouktif, S.; Fiaz, A.; Ouni, A.; Serhani, M.A. Optimal deep learning lstm model for electric load forecasting using feature selection and genetic algorithm: Comparison with machine learning approaches. *Energies* **2018**, *11*, 1636. [CrossRef]
34. Mu, H. Research on Robustness State of Charge Estimation of Lithium-Ion Power Battery for Electric Vehicles. Ph.D. Thesis, Beijing Institute of Technology, Beijing, China, 2016.

35. Mu, H.; Xiong, R.; Sun, F. A novel multi-model probability based battery state-of-charge fusion estimation approach. *Energy Procedia* **2016**, *88*, 840–846. [CrossRef]
36. Lin, C.; Mu, H.; Xiong, R.; Shen, W. A novel multi-model probability battery state of charge estimation approach for electric vehicles using H-infinity algorithm. *Appl. Energy* **2016**, *166*, 76–83. [CrossRef]
37. Lin, C.; Mu, H.; Xiong, R.; Cao, J. Multi-model probabilities based state fusion estimation method of lithium-ion battery for electric vehicles: State-of-energy. *Appl. Energy* **2017**, *194*, 560–568. [CrossRef]
38. He, M.; Jiang, J.; Huang, G.; Liu, J.; Li, C. Disintegration of rocks based on magnetically isolated high voltage discharge. *Rev. Sci. Instrum.* **2013**, *84*, 024704. [CrossRef]
39. Brouwer, G.K.; Fokker, P.A.; Wilschut, F.; Zijl, W. A direct inverse model to determine permeability fields from pressure and flow rate measurements. *Math. Geosci.* **2008**, *40*, 907–920. [CrossRef]
40. Chen, Z.; Xu, T.; Gómez-Hernández, J.J.; Zanini, A. Contaminant Spill in a Sandbox with Non-Gaussian Conductivities: Simultaneous Identification by the Restart Normal-Score Ensemble Kalman Filter. *Math. Geosci.* **2021**, *53*, 1587–1615. [CrossRef]
41. Jou, Y.; Lin, Z.; Chen, F. Improved Design of Two-Channel Quadrature Mirror Filter Using Explicit Toeplitz Expressions. In Proceedings of the 2018 IEEE 7th Global Conference on Consumer Electronics (GCCE), Nara, Japan, 9–12 October 2018; pp. 1–2.
42. Zhou, F.; Jiang, J.; Shui, P. Fast design of 2D fully oversampled DFT modulated filter bank using Toeplitz-block Toeplitz matrix inversion. *Signal Process* **2015**, *111*, 194–198. [CrossRef]
43. Sanjeevini, S.; Bernstein, D.S. Counting Zeros Using Observability and Block Toeplitz Matrices. *IEEE Trans. Autom. Control* **2020**, *66*, 1301–1305. [CrossRef]
44. Townsend, A.; Webb, M.; Olver, S. Fast polynomial transforms based on Toeplitz and Hankel matrices. *Math. Comput.* **2018**, *87*, 1913–1934. [CrossRef]
45. Gao, F.; Chi, H.; Shao, X. Forecasting residential electricity consumption using a hybrid machine learning model with online search data. *Appl. Energy* **2021**, *300*, 117393. [CrossRef]
46. Ghimire, S.; Deo, R.C.; Raj, N.; Mi, J. Deep solar radiation forecasting with convolutional neural network and long short-term memory network algorithms. *Appl. Energy* **2019**, *253*, 113541. [CrossRef]